ELSEVIER

Journal of Molecular Catalysis A: Chemical 155 (2000) 43–58

JOURNAL OF MOLECULAR CATALYSIS A: CHEMICAL

www.elsevier.com/locate/molcata

Silica-supported ytterbium oxide characterized by spectroscopic methods and acid-catalyzed reactions

Takashi Yamamoto *, Takahiro Matsuyama, Tsunehiro Tanaka, Takuzo Funabiki, Satohiro Yoshida

Department of Molecular Engineering, Graduate School of Engineering, Kyoto University, Kyoto 606-8501, Japan

Received 7 September 1998; accepted 1 February 1999

Abstract

Acid–base properties of silica-supported ytterbium oxide catalyst, loading amounts of which were 25 μmol–8.4 mmol Yb $g(SiO_2)^{-1}$, were investigated by TPD experiment and α-pinene isomerization. The relations among acid properties, structures, and catalytic properties are discussed. The catalytic activity depends on loading amounts of ytterbium and pre-treatment temperatures, and reached the highest when loading amount was 3.4 mmol $g(SiO_2)^{-1}$ and pre-treatment temperature of 1073 K. No crystalline phase was detected with XRD technique. By XAFS spectroscopy, Yb atoms adjacent to Yb were found to be absent, but the presence of Si atoms adjacent to Yb was observed in all the catalysts. XRD and XAFS analyses revealed that Yb atoms are supported on SiO_2 in a highly dispersed form as YbO_6 octahedra. Solid acidity is concluded to be due to strong interaction between a YbO_6 octahedron and a SiO_4 tetrahedron, and the specific activity per Yb–Si unit was independent of loading amounts. When loading amounts of Yb were excess to form two-dimensional ytterbium oxide overlayer, total turn over numbers were drastically reduced.

Keywords: Supported ytterbium oxide; SiO_2; Solid acid; α-Pinene isomerization; EXAFS

1. Introduction

The catalysis of rare-earth oxide is well-known, and many reactions have been reported [1–3]. Rare-earth oxide is known as a solid base catalyst, but there are few reports about catalysis over supported rare-earth compound. As a general use, rare-earth elements are added to catalyst supports to enhance their thermal stability [4]. Binary oxides of SiO_2–La_2O_3 and SiO_2–Y_2O_3 were predicted to exhibit acidity, according to the hypothesis proposed by Tanabe et al. [5,6]. Shen et al. [7] investigated acid–base property of europium oxides supported on silica and alumina by microcalorimetry and IR spectra of adsorption of ammonia and carbon dioxide. They observed a generation of base sites on alumina-supported europium oxide, whereas a generation of acid sites was observed on silica-

* Corresponding author. Fax: +81-75-753-5925; e-mail: yamamoto@dcc.moleng.kyoto-u.ac.jp

1381-1169/00/$ - see front matter
PII: S1381-1169(99)00318-0

supported europium oxide. Connell and Dumesic [8] reported the generation of Lewis and Brønsted acid sites on Sc/SiO_2 with IR spectra of adsorbed pyridine. However, catalytic reactions have not been performed in these works mentioned above. Recently, Soled et al. [9] reported the catalysis by rare-earth oxide loaded on silica–aluminas, acid strength of which was the same level as halide-treated aluminas. However, their aim was to control the acidity of silica–alumina by reduction of acid strength. Therefore, the relations among acid–base properties, structures, and catalytic properties of supported rare-earth oxide have been left unclear.

In the series of rare-earth elements, we paid attention to ytterbium. Kobayashi and Hachiya [10] reported that lanthanide trifluoromethanesulfonate acts as a water-tolerant Lewis acid, and the ytterbium triflate exhibited the highest activities in lanthanide triflates. Imamura et al. [11–13] and Baba et al. [14–16] prepared various kinds of supported Yb-amide complexes, which were prepared by impregnation of support-materials with a liquid ammonia solution of Yb metal, followed by evacuation. They reported that supported Yb(III)-amide complexes successively changed to Yb(II)-imide and finally to Yb(III)-nitride as ramping evacuation temperatures. The catalytic properties exhibited by these complexes were quite different from each other. In the case of Y-type zeolite supported Yb complex, Yb(II)-imide complex promoted base-catalyzed reactions [14,16]. In the case of Yb-dosed SiO_2, the atomic array of $\equiv Si–O–Yb–NH_2$ was responsible for hydrogenation property [12].

However, catalysis by supported ytterbium oxide has not been reported. We prepared silica-supported ytterbium oxide catalysts with various loading amounts of Yb by conventional impregnation method. In this work, we report acid–base property of silica-supported ytterbium oxide catalysts and the results of characterization of their structure. For the model reaction for acid–base property, α-pinene isomerization was utilized.

2. Experimental

SiO_2 gel was synthesized from tetraethyl orthosilicate (Nacalai tesque, EP-grade, once distilled) by hydrolysis in a water–ethanol mixture at boiling point followed by calcination at 773 K for 5 h in a dry air stream. Before calcination, a dried sample was ground to powder under 100 mesh. Silica-supported ytterbium oxide catalyst was prepared by impregnation of aqueous solution of ytterbium nitrate (Mitsuwa, 99.9%) to SiO_2 gel at 353 K. The sample was dried at 363 K for 12 h followed by calcination in a dry air stream at 773 K for 5 h. These samples are referred to as x mmol Yb/SiO_2 (x stands for loading amounts of Yb atom per 1 g of SiO_2). Ytterbium oxide was prepared by thermal decomposition of ytterbium nitrate at 773 or 1273 K for 5 h. They were identified by XRD patterns in comparison with C-rare-earth structure of Yb_2O_3 (JCPDS file No. 18-1463).

α-Pinene isomerization was carried out under dry N_2 atmosphere using a stirred batch reactor at 323 K. Before reaction, each sample was evacuated at 1073 K for 0.5 h and calcined under 6.66 kPa of O_2 for 1 h, followed by evacuation at the same temperature for 1 h. In a typical experiment, the reactor was loaded with 2 ml (12.6 mmol) of α-pinene (Nacalai, EP, 99.8%) and 50 mg of catalyst. Products were analyzed by GC and GC-Mass (Shimadzu, GCMS-QP5050).

BET specific surface area measurements were carried out with N_2 adsorption isotherms at 77 K. Each sample was pre-treated in the same as above.

Temperature-programmed desorption (TPD) experiment was used as a detector for quadrupole-type mass spectrometer. NH_3 and CO_2 TPD measurements were performed at a heating rate of 5 K min^{-1}, and TPD measurement of pyridine was performed at a heating rate of 10 K min^{-1}. The pre-treatment procedure was the same as mentioned above. The sample (100 mg) was exposed to 500 μmol of CO_2 or NH_3 at 373 K for 30 min, or 80 μmol of pyridine at

423 K for 10 min, followed by evacuation at the same temperature for 1 h. The amounts of desorbed gases (CO_2; m/e = 44, NH_3; m/e = 16, pyridine; m/e = 52) were normalized to that of introduced Ar (m/e = 40) as an internal standard. Because the most intense signal for pyridine-mass spectrum was that of m/e = 52, we adopted profiles of m/e = 52 for acid properties of each catalyst.

X-ray diffraction patterns of samples were obtained with a Rigaku Geigerflux diffractometer using Ni-filtered Cu Kα radiation (1.5418 Å).

Yb–L_{III} edge X-ray absorption experiments were carried out at BL10B, Photon Factory in High Energy Accelerator Research Organization (KEK-PF; Tsukuba, Japan) with a ring energy of 2.5 GeV and a stored current, 250–280 mA, and at BL01B1, SPring-8 (Hyogo, Japan) with a ring energy of 8 GeV and a stored current, 16–20 mA. The X-ray absorption spectra were recorded by the EXAFS facilities installed on the BL10B and BL01B1 in transmission mode at room temperature with a Si(311) and Si(111) two-crystal monochromator, respectively. X-ray was detected with ion chambers filled with 100% N_2, which are flowing at atmospheric pressure. The lengths of the ion chamber for incident and transmitted X-ray detection were 17 and 31 cm, respectively.

Data reduction was performed using a FACOM M1800 computer of Kyoto University Data Processing Center. The normalization method has been previously reported in detail [17]. To curve-fitting analysis, the following EXAFS formula was applied.

$$k^3\chi(k) = \Sigma_j\left(k^2 N_j/R_j^2\right) A_j(k)\exp\left(-2\sigma_j{}^2k^2\right) \times \sin\left(2kR_j + \delta_j(k)\right) \quad (1)$$

where, k is the wavenumber of photoelectron, N_j the number of scattering atoms of the jth shell located at a distance of R_j from a Yb atom, A_j, the envelope function which includes backscattering amplitude and damping factor caused by inelastic loss during electron traveling, σ_j the Debye–Waller factor and δ_j the phase shift. For an oxygen atom scatter, A_j and δ_j were extracted from L_{III} edge EXAFS spectrum of C-type Yb_2O_3 crystal, and hence, σ_j corresponds to the relative Debye–Waller factor derived from that of the reference compound. In the extraction of these parameters, EXAFS spectrum of Yb_2O_3 prepared at 1273 K was used.

3. Result and discussion

3.1. Catalysis

It is known that α-pinene isomerization was one of the excellent test reactions for acid–base catalyst [18–20], and the products of α-pinene isomerization can be classified to three groups as shown in Scheme 1. The first group is β-pinene. The second group consists of bicyclic products (camphene, α-fenchene, etc.). The last group is composed of monocyclic products (limonene, terpinolene, α-terpinene, γ-terpinene, etc.). Over solid base catalysts such as MgO and SrO, only equilibrium between α-pinene and β-pinene should be observed [21]. In contrast, acid catalysts promote the reactions producing all the three groups and the selectivities of which depend on the maximum acid strength. Table 1 shows results of α-pinene isomerization over silica-supported ytterbium oxide catalyst. Yb/SiO_2 catalysts exhibited high activity, however, SiO_2 and Yb_2O_3 were inactive for this reaction at 323 K. Catalytic activities varied with Yb loading amounts. Catalytic activities per unit weight catalyst were enhanced as increasing Yb loading amounts and reached the highest when those were 3.4 through 5.8 mmol $g(SiO_2)^{-1}$. The selectivity was independent of loading amounts. The main products were limonene and camphene, and selectivities of which were ca. 70% and 20%, respectively. A selective formation of β-pinene from α-pinene occurs over solid bases, whereas β-pinene was

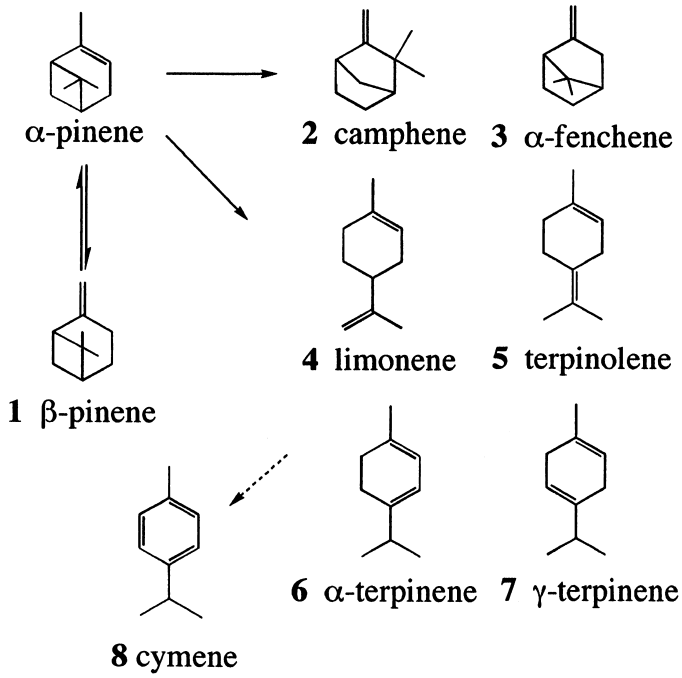

Scheme 1. α-Pinene isomerization.

scarcely produced over Yb/SiO_2 catalysts. The selectivities of Yb/SiO_2 catalysts for α-pinene isomerization indicate that the generated active sites were acid sites. The independence of selectivities to loading amounts was revealed that the acid strength distributions of all Yb/SiO_2 catalysts resemble each other. A difference of the selectivity for 280 μmol Yb/SiO_2 catalyst against others was only due to its low conversion of 1.3%.

To clarify the catalytic activity, we calculated specific activities per Yb atom from results of Table 1. The calculation was according to an assumption that all Yb-related sites of each catalyst participate in the catalysis. As shown in Fig. 1, estimated turn over numbers (TONs) per Yb atom are almost equal, except for 280 μmol and 8.4 mmol Yb/SiO_2 catalysts. This shows that each Yb-related site, loading amounts of which were among 1.7 and 5.8 mmol $g(SiO_2)^{-1}$, exhibits similar catalytic activities. The results that specific activity and the selectivity were quite similar indicate that the structure of active sites resembles each other.

Table 1
Results of α-pinene isomerization at 323 K[a]

Yb content		Conversion (%)	Selectivity[c] (%)							
mmol $g(SiO_2)^{-1}$	(wt.%)[b]		1	2	3	4	5	6	7	8
SiO_2		0								
0.0258	0.5	tr								
0.280	5.2	1.3	5	20	3	55	6	3	4	7
1.7	24.9	12.5	tr	26	2	62	4	2	2	2
3.4	39.8	26.5	tr	23	2	67	4	2	2	tr
3.8	42.9	20.9	tr	20	2	67	5	2	2	2
5.8	53.4	30.8	tr	20	1	68	5	2	2	2
8.4	62.3	5.5	tr	17	1	67	6	2	3	4
Yb_2O_3		0								
MgO[d]		2.1	100							tr

[a] α-Pinene, 2 m (12.6 mmol); catalyst, 50 mg; pre-treatment temperature, 1073 K; reaction time, 3 h.

[b] As Yb_2O_3.

[c] (1) β-Pinene, (2) camphene, (3) α-fenchene, (4) limonene, (5) terpinolene, (6) α-terpinene, (7) γ-terpinene, (8) others.

[d] Catalyst: 300 mg as $Mg(OH)_2$, pre-treatment temperature: 873 K, reaction temperature: 353 K.

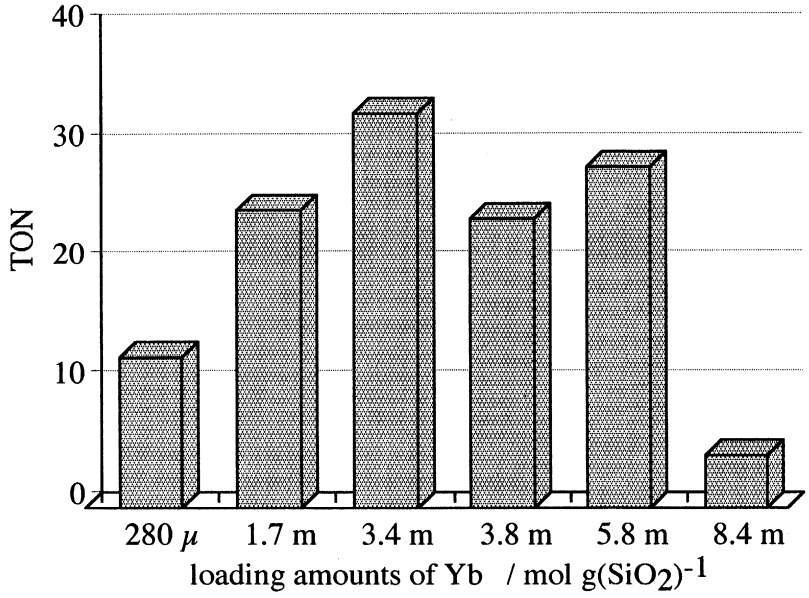

Fig. 1. TONs of catalysts in α-pinene isomerization. The TON per one Yb atom was calculated from results of Table 1.

The effect of pre-treatment temperature in α-pinene isomerization is shown in Fig. 2. We selected 3.4 mmol Yb/SiO_2 catalyst as a representative of silica-supported ytterbium oxide catalysts because the catalyst exhibited the highest catalytic activity. Catalytic activity strongly depends on pre-treatment temperature and the highest activity was exhibited when a catalyst was pre-treated at 1073 K. When the pre-treatment was carried out at 1273 K, the catalytic

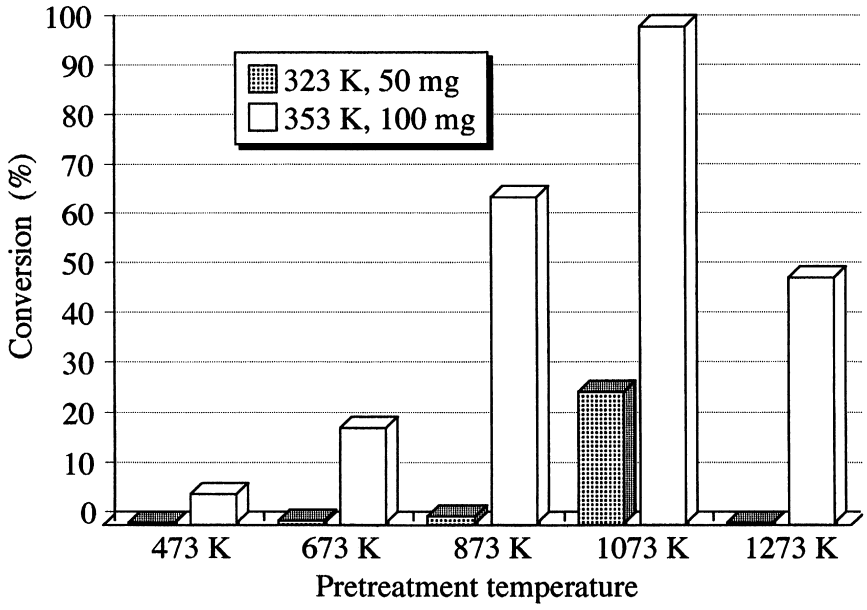

Fig. 2. Dependence of pre-treatment temperature in α-pinene isomerization. Catalyst: 3.4 mmol Yb/SiO_2, α-pinene: 2 ml, reaction time: 3 h.

activity was drastically reduced. To clarify the effect of pre-treatment temperature to catalysis, concentrations of products vs. that of α-pinene during reaction are plotted in Fig. 3. Although pre-treatment and reaction temperatures were variant for each plot, plots of all product concentrations, vs. that of α-pinene were on line except for α-fenchene and cymene. The slope of the lines for each product represents the selectivity for α-pinene isomerization. Those of limonene and camphene were 0.62 and 0.19, respectively, and these were almost the same as the results found in Table 1. This shows that the products selectivities of α-pinene isomerization independent of pre-treatment temperatures, and these compounds are the primary products. The concentration of cymene rapidly increased when α-pinene was almost consumed. This shows that cymene was the second product formed by dehydrogenation of monocyclic products such as limonene [18], terpinolene and α-, γ-terpinene [22].

The independence of selectivities to pre-treatment temperatures also revealed that the acid strength distributions resemble each other, the same as effects of loading amounts mentioned above. The same results were observed in the case of 1.7 mmol Yb/SiO_2 catalyst.

3.2. TPD

To examine acid–base property of catalysts, CO_2 and NH_3-TPD were carried out and the profiles are shown in Fig. 4. Much amount of CO_2 was desorbed from Yb_2O_3, whereas 3.4 mmol Yb/SiO_2 and SiO_2 did not desorb CO_2 at all. Basicity of ytterbium oxide completely disappeared in Yb/SiO_2 catalyst. In NH_3-TPD profiles, 3.4 mmol Yb/SiO_2 exhibited much larger peak around 473 K than Yb_2O_3 and SiO_2. It shows a generation of new acid sites over Yb/SiO_2 catalyst. On the other hand, another desorption peak above 573 K was observed on both Yb_2O_3 and SiO_2. It has been reported that rare-earth oxide possesses not only basic sites but also acid sites [23,24]. The NH_3-TPD profile of Yb_2O_3 had a desorption peak at 473 K and a shoulder peak at 723 K, and the tendency resembles that previously reported [25]. The NH_3-TPD profiles revealed that Yb_2O_3 possesses both acid and base sites, but Yb_2O_3

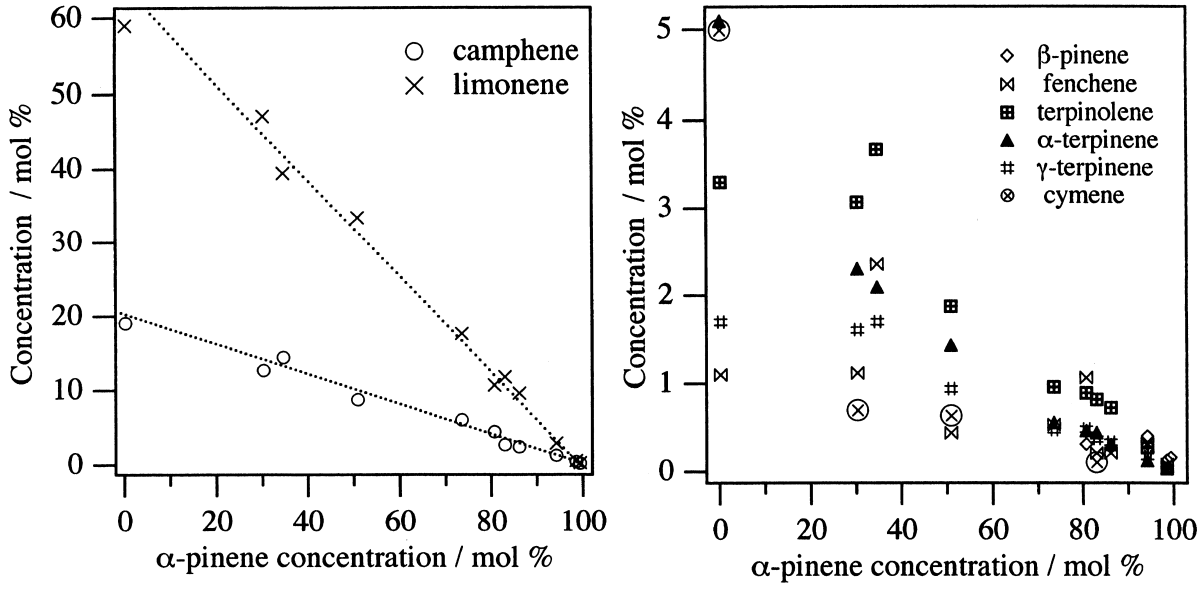

Fig. 3. Concentration of products vs. substrate in α-pinene isomerization. Plotted data are results of Fig. 2. Catalyst: 3.4 mmol Yb/SiO_2. Pre-treatment temperature: 473–1273 K. Reaction time: 323, 353 K.

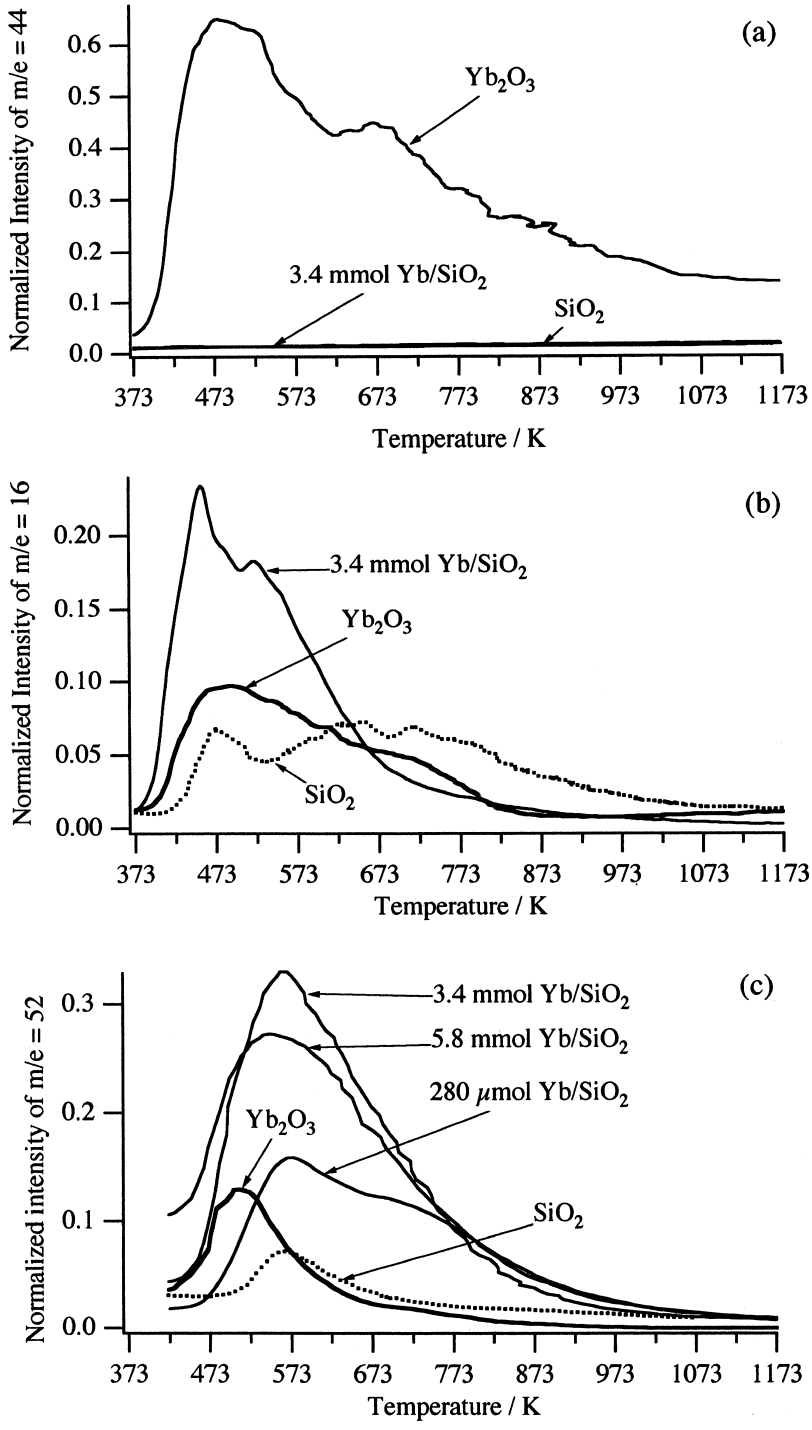

Fig. 4. TPD profiles of CO_2 (a), NH_3 (b), and pyridine (c). Pre-treatment procedure was performed at 1073 K.

pre-treated at 1073 K was inactive for α-pinene isomerization at 323 K.

From IR study, Morrow and Cody [26,27] have reported that silica evacuated above 673 K

has active siloxane bridge that reacts with NH_3 to produce $SiNH_2$ and SiOH at room temperature, whereas it did not react with pyridine. The desorption peak at around 623 K observed on silica was due to decomposition of surface $SiNH_2$ species. To clarify acidic property in more detail, pyridine TPD was also performed. Results were shown in Fig. 4c. The 3.4 mmol Yb/SiO_2 catalyst exhibited the largest peak at around 573 K in all the catalysts. The desorption peak of pyridine was observed on Yb_2O_3 and SiO_2, the same as those of NH_3-TPD measurements. However, the quantity of desorbed pyridine from Yb/SiO_2 catalysts extremely exceeded those of SiO_2 and Yb_2O_3. Results of pyridine TPD measurements correspond to catalytic results. In our case, pyridine TPD measurement is a more suitable method for an explanation of the acidic property than that of NH_3. In addition, the profile of SiO_2 exhibited only a single peak in contrast to that of NH_3. It is in agreement with IR study described above [26,27].

3.3. X-ray diffraction

Fig. 5 shows Cu Kα XRD patterns of catalysts pre-treated at 1073 K. Yb_2O_3 exhibited strong d_{222} and d_{400} reflections at 29.7° and 34.4°. SiO_2 gel exhibited a halo only around 22°. With increasing loading amounts of Yb, a new halo grew around 30°. This halo was due to amorphous phase of Yb_2O_3 or ytterbium silicate. Any distinct peak was not observed over all the catalysts, although loading amounts of ytterbium as Yb_2O_3 went up to 5–60 wt.%. This clearly shows that long-range ordering structures were not formed. A trace peak was observed on 8.4 mmol Yb/SiO_2 at 29.8°, which might be due to the d_{222} reflection of Yb_2O_3. However, large parts of Yb atoms of 8.4 mmol Yb/SiO_2 were present on SiO_2 in an amorphous phase because this peak was very faint and it was overlapping with a large halo.

In the phase diagram of Yb_2O_3–SiO_2 system, it was reported that Yb_2O_3 and SiO_2 does not form solid solutions but form crystals of $Yb_2O_3 \cdot SiO_2$ and/or $Yb_2O_3 \cdot 2SiO_2$ [28]. On the other hand, no crystalline phases were detected in all the catalysts. Therefore, it is concluded that ytterbium oxide on silica available for α-pinene isomerization is not in a crystal state but in an amorphous one.

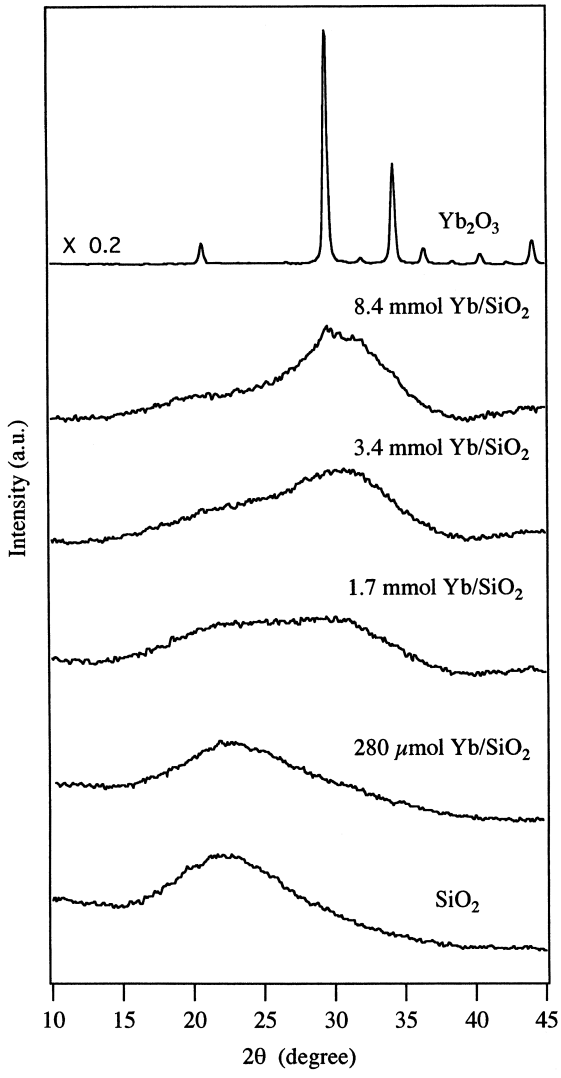

Fig. 5. Cu Kα XRD patterns.

3.4. X-ray absorption fine structure

Fig. 6 shows k^3-weighted EXAFS spectra and their Fourier transforms (FTs) of Yb_2O_3. In

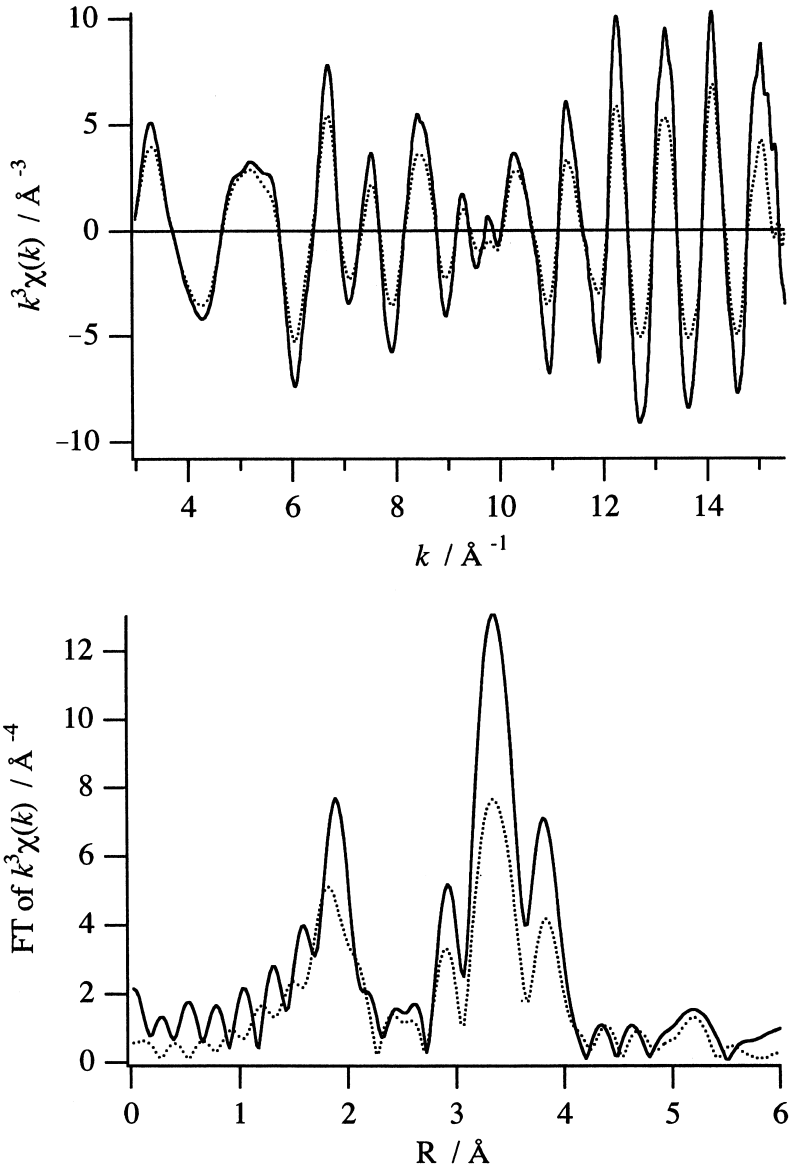

Fig. 6. XAFS spectra of Yb_2O_3. Solid curve: prepared by calcination of ytterbium nitrate at 1273 K. Dotted curve: calcined at 773 K.

the FT of EXAFS, peaks due to six O atoms and 12 Yb atoms were observed at 1.9 and 3.3 Å, respectively. These calculated distances from crystallographic data ($a_0 = 10.436$ Å), are 2.259 and 3.690 Å, respectively. The dotted curves in Fig. 6 are the spectra of the sample that was prepared by thermal decomposition of ytterbium nitrate at 773 K. The k^3-weighted EXAFS spectrum was quite similar to that of Yb_2O_3 prepared at 1273 K, although the amplitude was lower. It shows that ytterbium nitrate decomposed at 773 K and transformed to C-rare-earth structure of Yb_2O_3, although the crystallinity was relatively low. Therefore, all Yb atoms of catalysts were present on SiO_2 as oxide.

Fig. 7 shows Yb–L_{III} edge k^3-weighted EXAFS spectra of Yb/SiO_2 catalysts calcined at 773 K. The amplitudes and phases of all spectra

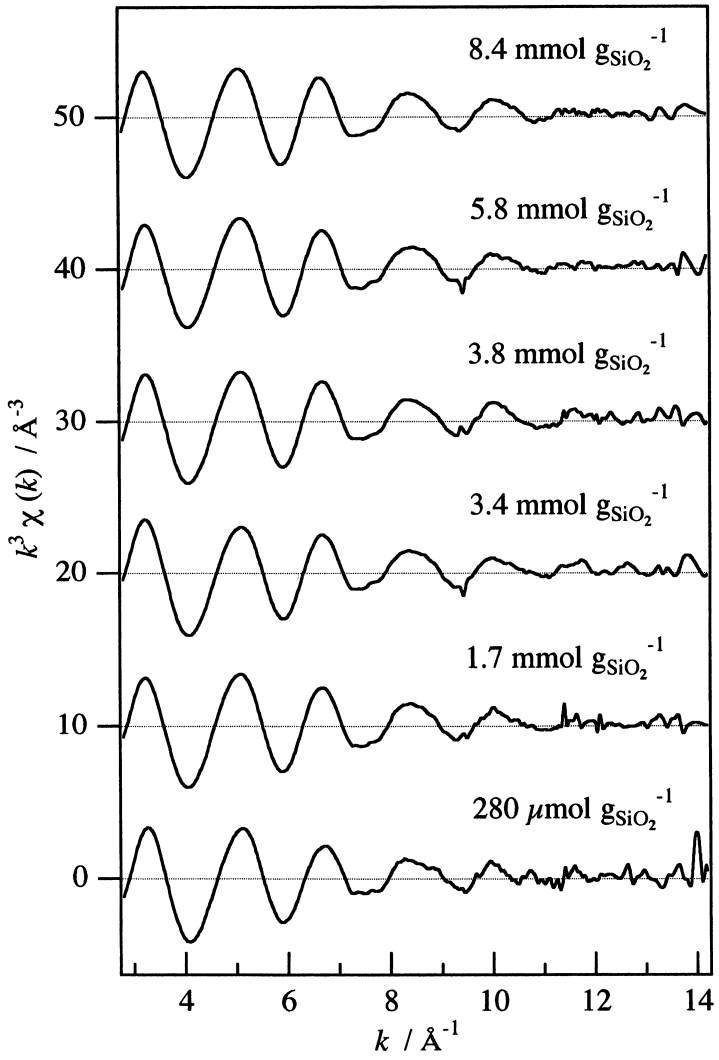

Fig. 7. k^3-Weighted Yb–L_{III} edge EXAFS spectra of silica-supported ytterbium oxide.

were quite similar to each other. The amplitude decayed with k increasing, and no oscillations were observed beyond 12 Å^{-1}. The similarity of each EXAFS spectrum indicates that the local structures around Yb were almost the same. The oscillation frequencies of one EXAFS spectrum were not constant, and it shows that the EXAFS spectrum consists of some sine waves, as noted in EXAFS formula (1). It is clear that neighboring atoms of Yb were not a single kind. Teo and Lee [29] calculated that backscattering amplitude functions of lanthanides have two peaks in low and high k region, and that of Yb has a large peak above 10 Å^{-1}. On the other hand, those of light elements such as O and Si are monotonously decreasing with k, and become very small above 10 Å^{-1}. Because the amplitude of EXAFS spectra of catalysts monotonously decayed with k, it was concluded that any Yb atoms did not present around an Yb atom, in contrast to Yb_2O_3.

The k^3-weighted Fourier transformation was carried out against EXAFS of catalysts in the k range of 3.0–15.0 Å^{-1}, to obtain the radial structure function (RSF). The results are shown in Fig. 8. In analogy with EXAFS spectra, all

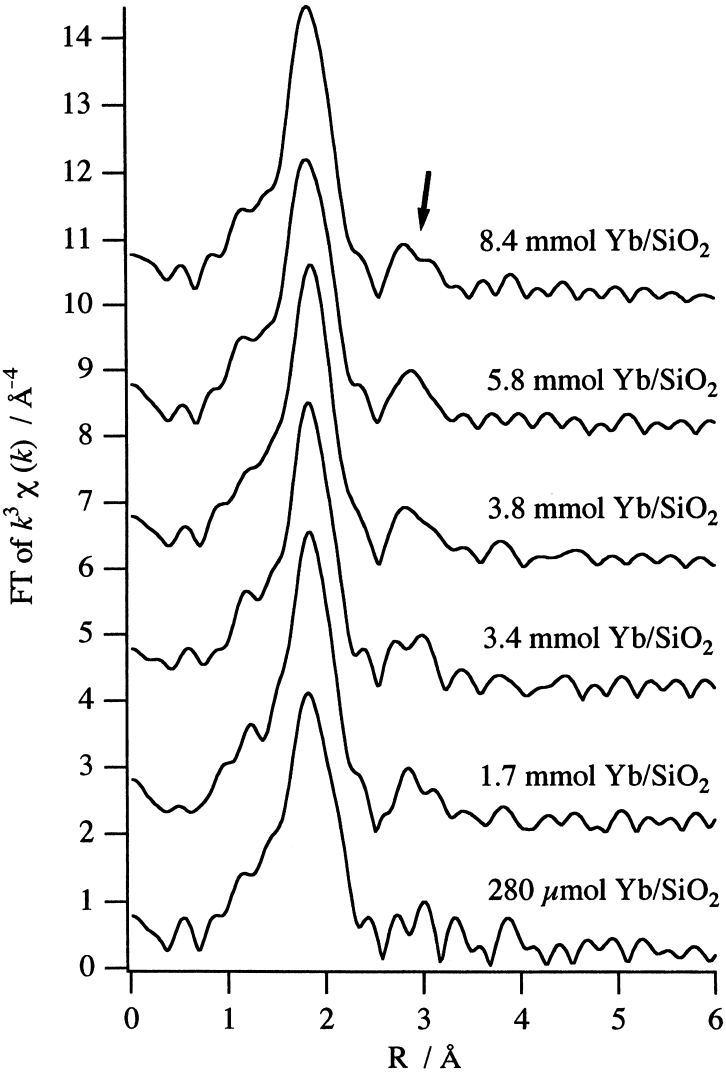

Fig. 8. FTs of k^3-weighted Yb–L_{III} edge EXAFS spectra of silica-supported ytterbium oxide.

RSF were quite similar, and two peaks were observed at around 1.8 and 2.9 Å. The peak at around 1.8 Å was due to O atoms, the distance of which was similar to that of Yb_2O_3. The distance of second peak (indicated by an arrow) was much shorter than the peaks due to Yb atoms in Yb_2O_3 crystal. From the EXAFS spectra, it is obvious that the second peaks are not due to heavy elements but due to light elements. As shown in Fig. 6, ytterbium nitrate was decomposed to Yb_2O_3 crystal even at 773 K. Then, we assigned the second peaks due to Si atoms of supports. The distance was similar to previously reported ones between Si and transition metal atoms, such as Ti [30], Ni [31], and Nb [32–35].

Fig. 9 shows Yb–L_{III} edge k^3-weighted EXAFS spectra variously treated Yb/SiO_2 catalysts, and Fig. 10 shows their FTs, Fourier ranges of which were 3.0–14.0 Å^{-1}. Each spectrum was also quite similar in these cases. This result indicates that any treatment did not effect the local structure around Yb, and long-range ordering structures have not been formed. The

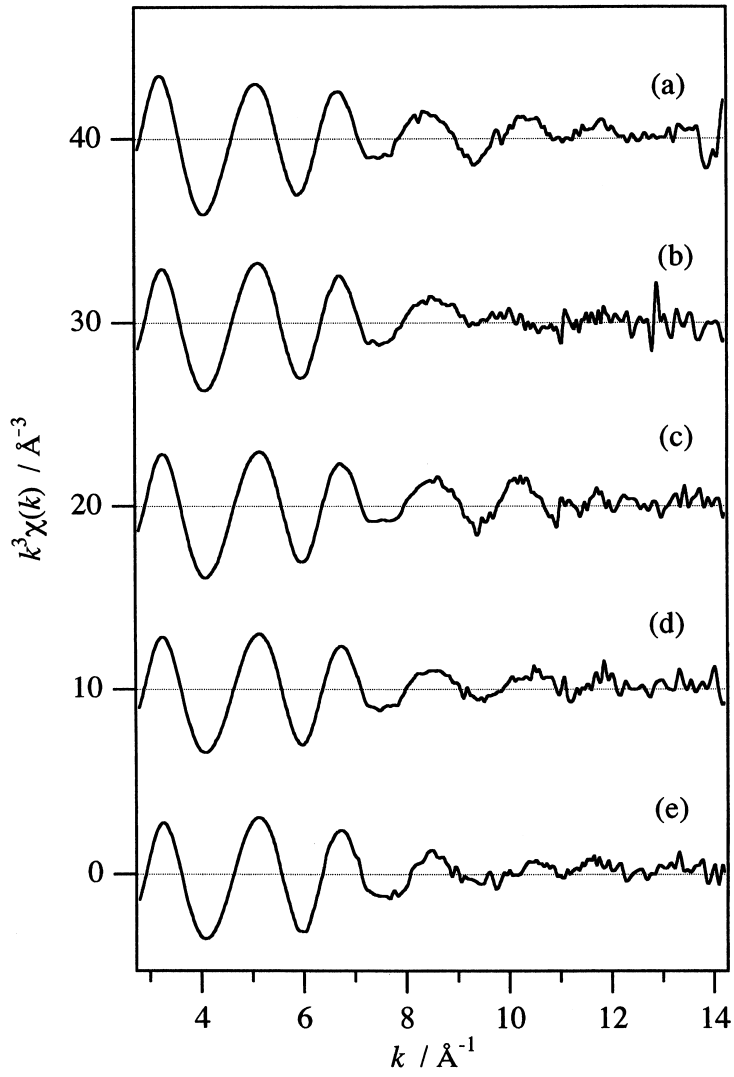

Fig. 9. k^3-Weighted Yb–L_{III} edge EXAFS spectra; 3.4 mmol Yb/SiO_2 calcined at 773 K (a), pre-treated at 1073 K (b), after reaction pre-treated at 1073 K (c), and pre-treated at 1273 K (d); 8.4 mmol Yb/SiO_2 pre-treated at 1073 K (e).

results of XRD measurements were supported by XAFS. In the FT of EXAFS functions, the magnitude of peaks due to Si (indicated by an arrow) were equal in all the catalysts independent of loading amounts and pre-treatment procedures. This shows that Yb atoms were supported on SiO_2 in a highly dispersed form, and the interaction between Si and Yb were strong.

The curve-fitting results of catalysts and the crystallographic datum of Yb_2O_3 are summarized in Table 2. The first coordination spheres of all the catalysts could be fitted by a single shell, and the estimated parameters were almost identical to each other. All the estimated parameters are consistent with those of Yb_2O_3 within an experimental error. The inter-atomic distances between Yb and O atoms strongly supported that Yb atoms of all the catalysts are in an octahedral coordination. From the results that no Yb–(O)–Yb contribution was observed and that of Yb–(O)–Si were observed, it is concluded that Yb atoms are supported on SiO_2 in

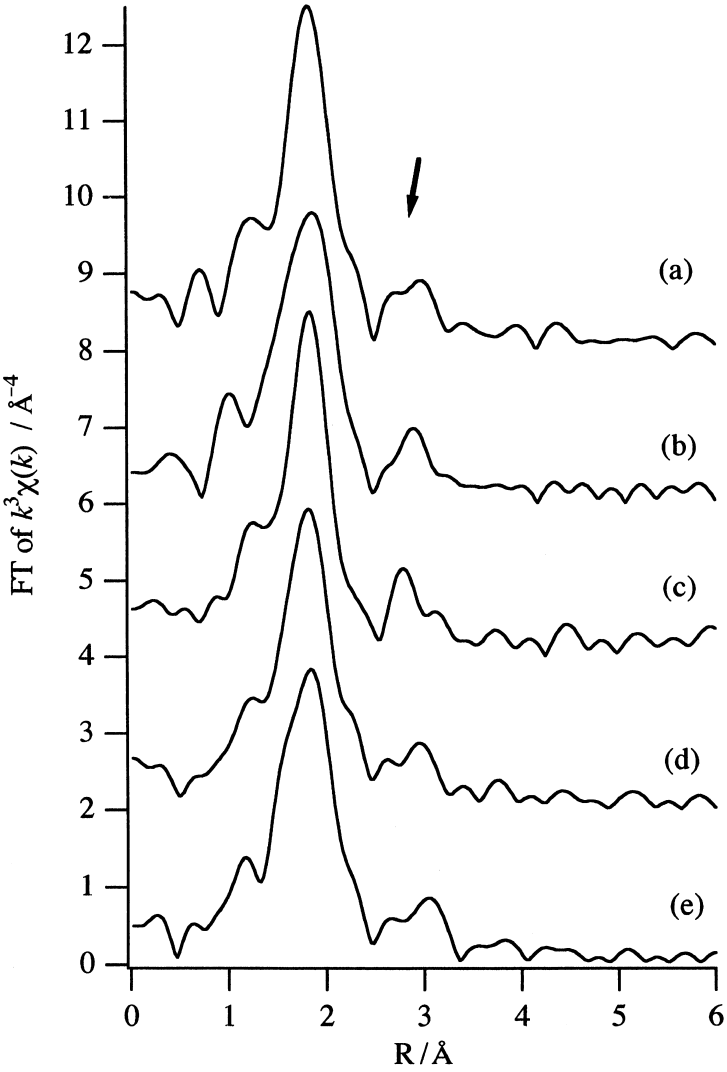

Fig. 10. FTs of k^3-weighted Yb–L_{III} edge EXAFS spectra; 3.4 mmol Yb/SiO_2 calcined at 773 K (a), pre-treated at 1073 K (b), after reaction pre-treated at 1073 K (c), and pre-treated at 1273 K (d); 8.4 mmol Yb/SiO_2 pre-treated at 1073 K (e).

a highly dispersed form as a YbO_6 octahedron, and a YbO_6 octahedron connect with SiO_4 tetrahedron through bridging oxygen. It is well-known that coordination environments of supported metal oxide often change by loading amounts and/or various treatments, and the changes of coordination cause the change of catalysis [36,37]. On the other hand, the coordination environments around Yb were independent of its loading amounts and pre-treatment procedures. This is the reason why no changes of its selectivity was observed in α-pinene isomerization.

3.5. Structure of active sites

Table 3 summarized the BET specific surface areas. The areas of catalysts include the SiO_2 carrier. The S_0 is a surface area $g(SiO_2)^{-1}$ carrier, which was calculated from BET specific surface area and Yb content. The $S_{occupied}$ is estimated occupied area by YbO_6 unit according

Table 2
Structural parameters for Yb–O shells of samples[a]

Sample	CN[b]	R (Å)[c]	$\Delta\sigma^2$ (Å^2)[d]	Refinement (%)[e]
Yb_2O_3	6	2.259		
280 μmol Yb/SiO_2	6.2	2.29	0.0048	5.8
1.7 mmol Yb/SiO_2	6.2	2.29	0.0032	5.1
3.4 mmol Yb/SiO_2[f]	6.0	2.29	0.0035	5.8
3.8 mmol Yb/SiO_2	5.7	2.29	0.0024	5.6
5.8 mmol Yb/SiO_2	5.9	2.28	0.0033	6.9
8.4 mmol Yb/SiO_2	6.1	2.29	0.0025	7.1
3.4 mmol Yb/SiO_2				
Fresh[f]	6.0	2.28	0.0032	9.2
Pre-treated at 1073 K	6.0	2.27	0.0044	9.5
After reaction	5.3	2.27	0.0020	6.7
Pre-treated at 1273 K	5.7	2.27	0.0039	7.5
8.4 mmol Yb/SiO_2				
Pre-treated at 1073 K	6.0	2.27	0.0044	12.2

[a] Inverse-Fourier range, $\Delta R = 1.2$–2.2 Å; fitting range, $\Delta k = 4.0$–12.0 Å^{-1}.
[b] Coordination number.
[c] Distance between Yb and O atoms.
[d] Relative Debye–Waller factor against that of reference sample (Yb_2O_3).
[e] $\sqrt{\Sigma\left(k^3\chi_{\text{observed}} - k^3\chi_{\text{calculated}}\right)^2 / \Sigma\left(k^3\chi_{\text{obvious}}\right)^2} \times 100$.
[f] Same sample.

to three assumptions described below. The first assumption is that all Yb atoms exist as a YbO_6 octahedron. The second is that all YbO_6 units have the same cross-section. The third assumption is that the cross-section is 16.0 Å^2 per YbO_6 unit, which is calculated by the following equation: $2.26 \times 2.26 \times \pi$.

The BET specific surface area gradually decreased with an increasing Yb loading amounts, and the surface area of carrier also decreased. In the case of 3.4 mmol Yb/SiO_2 catalyst, the surface area pre-treated at 1073 K kept 85% of that pre-treated at 673 K (fresh catalyst), whereas that pre-treated at 1273 K was reduced to 50% of the original by sintering. This abrupt decrease of surface area between 1073 and 1273 K is one of the reasons for deactivation of catalyst, as shown in Fig. 2. Because the extent of deactivation exceeded that of sintering, another factor for deactivation should be considered although it is not clear now.

As shown in Fig. 1, the high catalytic activities per Yb atom were demonstrated when loading amounts of Yb were among 1.7 and 5.8 mmol $g(SiO_2)^{-1}$. In cases of these loading amounts, the areas occupied by YbO_6 units (S_{occupied}) were calculated to be 162–559 m^2 $g(SiO_2)^{-1}$. These values were comparable to

Table 3
Physical properties of samples

Yb content		Pre-treatment temperature (K)	Area[b] (m^2 g^{-1})	S_0^c (m^2)	S_{occupied}^d (m^2 $g(SiO_2)^{-1}$)
mmol $g(SiO_2)^{-1}$	(wt.%)[a]				
SiO_2		673	661	661	
		1073	601	601	
0.0258	0.5	1073	597	600	2.5
0.28	5.2	1073	501	528	27
1.7	24.9	1073	321	427	162
3.4	39.8	473	206	342	323
		673	212	352	323
		873	199	331	323
		1073	180	299	323
		1273	104	173	323
3.8	42.9	1073	145	253	368
5.8	53.4	1073	108	231	559
8.4	62.3	1073	50	132	812
Yb_2O_3[e]		673	45		
		1073	16		

[a] As Yb_2O_3.
[b] BET specific surface area.
[c] Surface area of $g(SiO_2)^{-1}$ carrier.
[d] Occupied area by assumed YbO_6 unit.
[e] Prepared by thermal decomposition of ytterbium nitrate at 773 K for 5 h.

surface areas of $g(SiO_2)^{-1}$ carriers and the area of SiO_2 pre-treated at 1073 K. It shows that two-dimensional thin-layers of ytterbium oxide were formed on the SiO_2 surface, and the local interaction between a YbO_6 octahedron and a SiO_4 tetrahedron caused solid acidity. In the case of 8.4 mmol Yb/SiO_2, the calculated $S_{occupied}$ is 812 m^2 $g(SiO_2)^{-1}$, which exceeds the area of carrier. The excess Yb atoms were deposited on the thin-layer and blocked active sites, the same as zirconium oxide deposited on TiO_2 [38]. Therefore, the estimated specific activity per Yb atom of 8.4 mmol Yb/SiO_2 was quite low. Because the highest activity was exhibited when pre-treatment procedure was performed at 1073 K, we propose that the active sites are Lewis acid sites. It was reported that silica monolayer deposited on metal oxide exhibits weak Brønsted acidity [39–42], and niobium oxide one-atom-layers on SiO_2 catalyzes dehydration of ethanol [33]. In the case of Yb/SiO_2 catalysts, it is concluded that the analogous two-dimensional ytterbium oxide overlayers were formed in 5.8 mmol Yb/SiO_2. The reason for no Yb–(O)–Yb configuration was observed in XAFS spectra is as follows; the distributions of distances among Yb atoms were wide and the Debye–Waller factor of Yb–Yb bonding due to static structural disorder was extremely large. In the case of 1.7 mmol Yb/SiO_2, the loading amount of Yb was much less than a formation of YbO_6 monolayer, but the specific activity per Yb atom was comparable to that of 5.8 mmol Yb/SiO_2. It shows that the formation of ytterbium oxide monolayer was not necessary for the generation of acid sites. It was concluded that the generation of solid acidity over Yb/SiO_2 catalyst was due to the strong interaction between a YbO_6 octahedron and a SiO_4 tetrahedron.

4. Conclusion

Silica-supported ytterbium oxide catalyst exhibit a solid acidity and catalyzes α-pinene isomerization. The selectivity is independent of loading amounts and pre-treatment temperature. The highest activity is exhibited when pre-treatment is performed at 1073 K. Catalytic activity per Yb atom is constant when loading amounts are below 5.8 mmol $g(SiO_2)^{-1}$. Ytterbium atoms are widely spread on SiO_2 surface as a YbO_6 octahedron, and the YbO_6 octahedron strongly interacts with SiO_4 tetrahedron. Local interaction between silica and ytterbium oxide generates solid acidity.

Acknowledgements

This work has been performed under the approval of the Photon Factory Program Advisory Committee (Proposal No. 95G201), and SPring-8 Users Office (Japan Synchrotron Radiation Research Institute) (Proposal No. 1997B0071-NX -np). We are indebted to Prof. M. Nomura (KEK-PF) in carrying out the X-ray measurements. We thank Drs. S. Emura (Osaka University), Y. Nishihata (JAERI), H. Tanida (RIKEN), and T. Uruga (SPring-8) for making the XAFS beam of SPring-8 BL01B1 available. This work was partially supported by a grant-in-aid (No. 08405052) from Japan Ministry of Education, Science, Sports, and Culture.

References

[1] M.P. Rosynek, Catal. Rev. -Sci. Eng. 16 (1977) 111.
[2] K. Tanabe, M. Misono, Y. Ono, H. Hattori, New Solid Acids and Bases, Kodansha, Elsevier, Tokyo, 1989, pp. 41–47.
[3] K. Otsuka, K. Jinno, A. Morikawa, J. Catal. 100 (1986) 353.
[4] H. Arai, M. Machida, Appl. Catal., A: General 138 (1996) 161, and references therein.
[5] K. Tanabe, T. Sumiyoshi, K. Shibata, T. Kiyoura, J. Kitagawa, Bull. Chem. Soc. Jpn. 47 (1974) 1064.
[6] K. Tanabe, M. Misono, Y. Ono, H. Hattori, New Solid Acids and Bases, Kodansha, Elsevier, Tokyo, 1989, pp. 108–111.
[7] J. Shen, M.J. Lochhead, K.L. Bray, Y. Chen, J.A. Dumesic, J. Phys. Chem. 99 (1995) 2384.
[8] G. Connell, J.A. Dumesic, J. Catal. 105 (1987) 285.
[9] S.L. Soled, G. McVicker, S. Miseo, W. Gates, J. Baumgartner, Stud. Surf. Sci. Catal. 101 (1996) 563.
[10] S. Kobayashi, I. Hachiya, J. Org. Chem. 59 (1994) 3590.

[11] H. Imamura, H. Yoshimochi, Y. Sakata, S. Tsuchiya, J. Mol. Catal. 66 (1991) L33.
[12] H. Imamura, T. Konishi, Y. Sakata, S. Tsuchiya, J. Chem. Soc., Faraday Trans. 88 (1992) 2251.
[13] H. Imamura, T. Konishi, E. Suda, Y. Sakata, S. Tsuchiya, Bull. Chem. Soc. Jpn. 69 (1996) 77.
[14] T. Baba, G.J. Kim, Y. Ono, J. Chem. Soc., Faraday Trans. 88 (1992) 891.
[15] T. Tanaka, T. Hanada, S. Yoshida, T. Baba, Y. Ono, Jpn. J. Appl. Phys. 32 (1993) 481.
[16] T. Baba, S. Hikita, R. Koide, Y. Ono, T. Hanada, T. Tanaka, S. Yoshida, J. Chem. Soc., Faraday Trans. 89 (1993) 89.
[17] T. Tanaka, H. Yamashita, R. Tsuchitani, T. Funabiki, S. Yoshida, J. Chem. Soc., Faraday Trans. 1 84 (1988) 2987.
[18] R. Ohnishi, K. Tanabe, S. Morikawa, T. Nishizaki, Bull. Chem. Soc. Jpn. 47 (1974) 571.
[19] A. Corma, H. García, Catal. Today 38 (1997) 257.
[20] T. Yamamoto, T. Tanaka, T. Funabiki, S. Yoshida, J. Phys. Chem. B 102 (1998) 5830.
[21] R. Ohnishi, K. Tanabe, Chem. Lett. (1974), 207.
[22] T. Tanaka, A. Itagaki, G. Zhang, H. Hattori, K. Tanabe, J. Catal. 122 (1990) 384.
[23] V.R. Choudhary, V.H. Rane, J. Catal. 130 (1991) 411.
[24] G.A.M. Hussein, B.C. Gates, J. Chem. Soc., Faraday Trans. 92 (1996) 2425.
[25] V.R. Choudhary, V.H. Rane, J. Catal. 130 (1991) 411.
[26] B.A. Morrow, I.A. Cody, J. Phys. Chem. 80 (1976) 1995.
[27] B.A. Morrow, I.A. Cody, J. Phys. Chem. 80 (1976) 1998.
[28] E.M. Levin, C.R. Robbins, H.F. McMurdie, Phase Diagrams for Ceramists, The American Ceramic Society, Columbus, OH, 1969, p. 108, Fig. 2391.
[29] B.-K. Teo, P.A. Lee, J. Am. Chem. Chem. 101 (1979) 2815.
[30] S. Yoshida, S. Takenaka, T. Tanaka, H. Hirano, H. Hayashi, Stud. Surf. Sci. Catal. 101 (1996) 871.
[31] J.Y. Carriat, M. Che, M. Kermarec, M. Verdaguer, A. Michalowicz, J. Am. Chem. Soc. 120 (1998) 2059.
[32] M. Nishimura, K. Asakura, Y. Iwasawa, Proc. 9th. Int. Congr. Catal., Calgary, 1988, p. 1842.
[33] K. Asakura, Y. Iwasawa, J. Phys. Chem. 95 (1991) 1711.
[34] N. Ichikuni, Y. Iwasawa, Catal. Today 16 (1993) 427.
[35] H. Yoshida, T. Tanaka, T. Yoshida, T. Funabiki, S. Yoshida, Catal. Today 28 (1996) 79.
[36] S. Yoshida, T. Tanaka, in: Y. Iwasawa (Ed.), X-ray Absorption Fine Structure for Catalysts and Surfaces, World Scientific, Danvers, 1996, pp. 304–325.
[37] K. Asakura, Y. Iwasawa, in: Y. Iwasawa (Ed), X-ray Absorption Fine Structure for Catalysts and Surfaces, World Scientific, Danvers, 1996, pp. 192–215.
[38] T. Tanaka, T.M. Salama, T. Yamaguchi, K. Tanabe, J. Chem. Soc., Faraday Trans. 86 (1990) 467.
[39] M. Niwa, N. Katada, Y. Murakami, J. Phys. Chem. 94 (1990) 6441.
[40] M. Niwa, N. Katada, Y. Murakami, J. Catal. 134 (1992) 340.
[41] N. Katada, T. Toyama, M. Niwa, J. Phys. Chem. 98 (1994) 7647.
[42] T.-C. Sheng, I.D. Gay, J. Catal. 145 (1994) 10.